Experimental characterization of TIAGO torch discharges: surface wave discharge behavior and (post-)discharge kinetics.

Authors: Information avoided to favor the anonymizing process.

Affiliation: Information avoided to favor the anonymizing process.

ABSTRACT

The *Torche à Injection Axial sur Guide d'Ondes* source −better-known as TIAGO torch− is a particular type of Microwave Induced Plasma which has become in the technological and scientific spotlight due to its outstanding features. Moreover, TIAGO torch device arouses interest thanks to its remarkable performance in many challenging topics as green energy generation or graphene production by hydrocarbons decomposition. Although it has not been experimentally demonstrated up to date, discharges generated by a TIAGO torch have been theoretically predicted to be Surface Wave Discharges, a kind of plasmas leading the development of new materials. Therefore, a deeper and fundamental research of this device is needed to optimize the implementation of plasma technology to these fields. In this study, the axial distribution of gas temperature, electron density and intensity of main atomic and molecular emissions have been studied by Optical Emission Spectroscopy feeding the discharge with different input power values (200, 400 and 600 W). A complete axial characterization of both the dart and the plume regions is depicted and, according to the data obtained for the main plasma parameters, different regions can be identified, being the radiation zone reported for the first time at atmospheric pressure. The kinetics of both the dart and the plume are discussed and an experimental verification of the TIAGO torch behavior as a surface wave discharge is presented for first time.

1. INTRODUCTION

Despite being first reported in 1970 by Tuma [1], surface wave discharges (SWDs) are in the forefront of technological innovation contributing to the development of new advanced materials [2], the modification of material surfaces [3] and films [4] or green energy generation [5], among others. Therefore, it is not surprising that the most fundamental research of this special kind of microwave induced plasmas (MIPs) discharges keeps up to date [6-9].

Both surfatron and surfaguide are two of the most well-known electromagnetic field applicators for SWDs generation [10,11]. SWDs are sustained by a wave excited at a given point of a confining dielectric vessel which propagates through the plasma-dielectric interface while transferring energy to sustain the plasma. A SWD is characterized by an increase in its length with power supplied for its generation and a linear decrease of electron density along the discharge being its slope independent of power [12]. These discharges show some interesting advantages for the implantation of processes on the industry such as high reproducibility, versatility, stability, ease of manipulation [13] and the possibility to sustain them at atmospheric pressure. Furthermore, SWD features can be easily modified by changing external experimental conditions such as nature and flow of gas or applied microwave power which results in substantial variations on their performance in applications, *e.g.* in [14] an increase in the flow of the main gas reduced the amount of carbon-based material and gaseous-byproducts through the decomposition of organic precursor. Therefore, the knowledge and control of these features is highly interesting for the development of new applications.

Among MIPs generation devices, cavities, resonators or SWDs [10,15-21] should be highlighted. However, microwave torches stand out due to their ability to deliver higher powers to the discharge as compared to the abovementioned applicators. This higher power leads to larger electron density and temperatures values, thus favoring certain reactions for applications in different scientific and technological fields. An example of such devices is TIAGO torch (*Torche à Injection Axiale sur Guide d'Ondes*), developed by Moisan et *al*. [22] as an improvement of the well-studied TIA torch (*Torche à Injection Axiale*) [23]. Here below, these MIPs generation devices are briefly presented.

Both cavities and resonators are based on a simple principle to couple the energy of the electromagnetic field to the plasmas. They take advantage of a cavity-specific resonance mode of the electromagnetic field to couple the energy in the most efficient way to the discharge. These devices can work at both low or high pressures and can be coupled to setups as nebulizers or gas chromatographs, being their main restrictions of geometric type. The Beenaker cavity [16] is undoubtedly the most utilized of this kind of devices.

The propagation of surface waves has been extensively studied in the literature. In [24], Margot and Moisan examined the influence of collisions on the surface wave

propagation along a plasma column in vacuum, discussion easily extended to the case of a plasma column enclosed in a dielectric material, and they proved that only in absence of collisions the wave propagates entirely along the axial direction. In the case of collisions taking place with a non-negligible frequency, the higher the collision frequency, the more the directions of wave propagation. Keeping up with this topic, in [25] Grosse et *al.* analyzed simultaneous effects of collisions and inhomogeneity of plasmas on the surface wave and it was found that not only collisionality, but also inhomogeneity has a strong influence on the phase diagram of the wave propagation along a plasma column confined in a glass dielectric tube. For noteworthy inhomogeneities, as in the case of low densities at the interface between discharge and surroundings, local plasmas resonances were evidenced to become possible, significantly modifying the curves for wavenumber as well as damping coefficient. Later, Nowakowska et *al.* [26] first showed theoretically that the electromagnetic wave propagating along a dense plasma filament was a surface wave. The radial distribution of the electromagnetic field intensity was analyzed showing that it is mainly concentrated at the interface between the plasma and the surrounding air which acts as an effective dielectric cylinder. Afterwards, Zhang et *al.* [27] drawn some conclusions that are valid for Ar plasmas, but also, at least, for air, He, Ne and carbon dioxide plasmas. It was found that (i) increasing the gas flow rate leads to a decrease of the surface wave propagation distance in the gas inlet direction, (ii) the shortening of plasma column length with an increase of the gas entrance is supported by the decrease of the surface wave propagation distance and (iii) when the main gas flow is high enough, discharge instabilities and eventual extinction of the plasma are caused by the disappearance of the travelling surface wave in the cylindrical discharge tube. Furthermore, surface waves propagation at low pressure has also been deeply studied [28-30], but it is out of the scope of this work.

The last of the abovementioned MIPs devices are plasma torches, which are the focus of the present work. TIAGO torch field applicator creates a flame-like discharge generated at the tip of a nozzle. These discharges can be obtained inside a cylindrical glass reactor coaxially placed around the nozzle, with an outflow opened to allow working at atmospheric pressure and with or without shielding the radiation. In this way, the flame is surrounded by the reactor-contained air, presenting two different luminous regions: a bright filamentary plasma column (dart) and a less intense, broader shell region (plume) that extends beyond the plasma dart. Recently, Moisan and Nowakowska [6] suggested

that both TIA and TIAGO torch discharges consist of a SWD guided through the plasma-air interface with the surrounding air acting as a virtual cylindrical dielectric vessel for the propagation of the electromagnetic wave surface [6,22,26]. Other theoretical studies have also shown this behavior. For example, in [31] Alves et *al.* demonstrated that the electromagnetic field in a TIA torch discharge is maximum at the radial interface between plasma and atmosphere which, as it has been previously indicated, it is a characteristic feature of SWDs. Concerning the experimental demonstration of microwave plasma torch plasmas behaving as SWDs, unfortunately, neither a complete evidence nor a direct identification of this behaviour is found in literature; *e.g.* in [32] and [33] a linear decrease of electron density is showed when moving far from the field applicator along plasma discharge, however, a formal and complete experimental proof of being a SWD is not presented.

In [32,34], TIAGO torch discharges were experimentally studied, including the conditions for appropriate torch operation, flame morphology and the interaction of the torch flame with the surrounding atmosphere, using several gas-flow rates and microwave input powers. Besides, gas temperature and electron density values were also measured using optical emission spectroscopy techniques, revealing that the dependence of these parameters on input power was not as important as on gas flow rate.

Although TIAGO torch source has been found to be of special interest for the generation of green hydrogen [35] and few layers graphene nanosheets [36,37] by ethanol decomposition, fundamental research of these plasmas −*i.e.* discharge kinetics, morphology…− would facilitate the optimization of this technology. For instance, for graphene synthesis, Tsygonov et *al.* [38] modeled the decomposition of ethanol molecules in surface wave-based discharges in a region named *hot plasma zone,* whereas the formation of graphene flakes occurs in the *assembly* or *nucleation region*. Snirer et *al*. [39] experimentally verified the existence of those regions for graphene formation in a microwave plasma torch. Besides, in [40] it was demonstrated the influence of experimental conditions on the morphology of those regions which turned crucial for the amount and defectiveness formation of graphene nanosheets. Therefore, deeper research on the characterization of the dart and plume regions of TIAGO torch in terms of kinetics and surface wave discharge features for the optimization of its applications, and particularly graphene formation, is fundamental.

In this paper, first experimental verification of the behavior of plasmas generated by the TIAGO torch as a SWD is sought by performing an axial characterization of both the dart and the plume regions. To that end, the axial distribution of electron density and gas temperature along the axial direction of the discharge have been studied by spectroscopic methods as a function of the input power. These data allow, for the first time, for characterizing the plume zone and discussing the different kinetics of both the dart and plume regions which will give valuable information for the optimization of TIAGO torch applications such as the formation of graphene nanosheets.

2. EXPERIMENTAL SETUP AND METHODS

Figure 1 shows a schematic diagram of the plasma source and the optical device used in this study. The plasma was created using a TIAGO torch device [22], whose detailed description can be found in [34]. A cylindrical glass reactor, like the one used in [34], was placed around the torch. The reactor was equipped with a quartz window to allow registering the discharge-emitted radiation while avoiding radiation absorption in the UV-region (< 400 nm). The reactor had three outflows: one coaxial with the discharge placed at the top and the other two located perpendicularly to the axis of the discharge. During the experiments reported herein, only the outflow on the top was left open for gas evacuation purposes, thus allowing to work at atmospheric pressure as it can be observed in the photograph of the reactor in Figure 1.

According to previous experimental results [34], larger argon gas flows resulted in a lower influence of the surrounding atmosphere on the plasma dart, as well as in longer darts, thus allowing for a more detailed axial study. Therefore, for all the experiments, a flow of 5.00 slm (*standard liter per minute*) of high purity argon (99.999%, Linde) was used to feed the torch. The flow was kept steady using mass-flow controllers (HI-TEC IB31, Bronkhorst). In this research, powers of 200, 400 and 600 W were used to sustain the plasma. Microwave (2.45 GHz) power was provided by a generator (GMP KG/D, Sairem) able to supply up to 2000 W in continuous mode, equipped with a water-cooled circulator to avoid power reflection damage. A triple stub was used to keep the reflected power lower than 5% of incident power at any time.

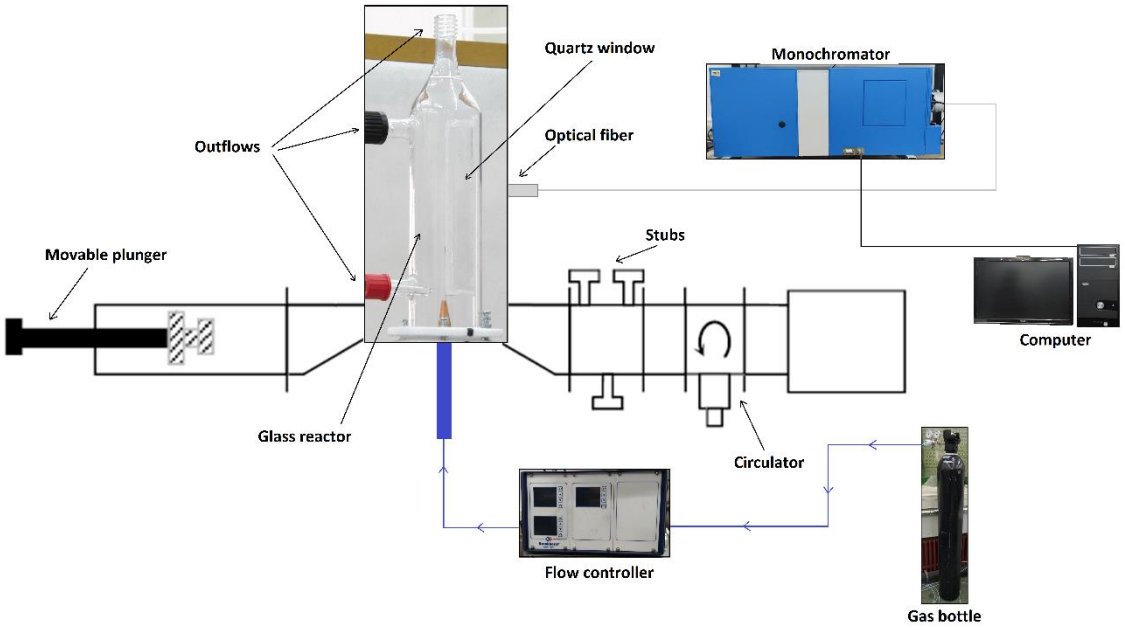

Figure 1. Experimental setup

Dart – and plume – emitted radiation was taken by an optical fiber placed perpendicularly to the axial direction of the reactor and equipped with a collimator allowing for 1-mm spatial resolution. The fiber was placed 3 cm away from the center of the reactor behind its wall. For each power, the fiber was moved along the axial direction (y—axis) of the dart (Figure 2) using a micrometer screw. Therefore, species from both the plasma dart and the plume were identified and axial profiles of plasma parameters (electron density and gas temperature) were obtained. Axial distances, y, were measured considering the tip of the nozzle as the initial position ($y = 0$). Moreover, to analyze the plasma behavior as a SWD (see Section 4), z distances were also measured considering the end of the dart as the initial position, $z = 0$ (Figure 2).

The radiation taken by the optical fiber was driven to the entrance slit of a previously calibrated in intensity Jobin-Yvon-Horiba monochromator (Czerny-Turner) of 1 m focal length, equipped with a 2400 grooves/mm holographic grating. Intensity calibration was performed using a GY 6.35 halogen lamp and the resolution of the spectrometer resulted in 4 pm. Instrumental width was determined by the full broadening at half height of the 632.80 nm spectral line of an He-Ne laser and resulted in 0.0208 ± 0.0003 nm for a slit width of 50 µm. A Hamamatsu R928P photomultiplier and a Symphony CCD camera (1024x256-OPEN-SITE) were used as radiation detectors. The optical system was completed with a SpectrACQ2 unit acting as interface between the

computer and the monochromator. Synergy data acquisition software allowed for choosing the detector, spectral range, exposition time, step length and photomultiplier voltage during measurements.

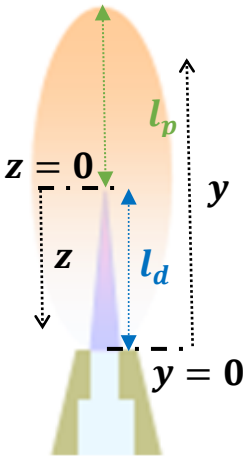

Figure 2. Graphic representation of different coordinates systems. Dart and plume lengths are also schematized (l_d and l_p, respectively).

The ro-vibrational spectra of different molecular species such as OH or N_2^+ are typically used to measure the plasma gas temperature (T_{gas}), assuming that their rotational kinetics is in equilibrium with the kinetic energy of heavy particles in the plasma. This assumption can be made in atmospheric pressure plasmas since the exchange between the translational energy of the molecules and their internal ro-vibrational states is very efficient [41]. In our case, the first negative system (FNS) of the nitrogen molecular ion (N_2^+) was utilized for this purpose, following the procedure described in [34].

Although atomic spectral lines of hydrogen Balmer series, which are frequently used to determine the value of electron density, can be observed due to impurities in Ar [42], when the argon plasma is open to the atmosphere, the interaction of nitrogen from the surrounding ambience with Ar discharge notably alters pure argon plasma kinetics and the emission of Balmer lines is not always detected as it has been previously reported for both TIAGO and TIA torches [34,43]. Therefore, electron density (n_e) was measured from the Stark broadening of the H_α line (623.3 nm) of the Hydrogen Balmer series instead of the most habitually used H_β line (486.1 nm) due to the no detection of the latter under the operational conditions used in our experiments. The same procedure described

in [32,34] was used to determine the Stark broadening of the H_α line. In the experimental conditions of this research, spectral lines can be fitted to a Voigt function [44] stemming from the convolution of both a Gaussian and a Lorentzian profile. Since natural broadening can be neglected, Gaussian width can be considered a contribution of instrumental and Doppler broadenings, while the Lorentzian width of the line can be calculated as a contribution of the Stark and the van der Waals broadenings. After the Lorentzian width is obtained, the van der Waals contribution [44] was determined and subtracted from it to determine the Stark broadening, from which n_e was calculated using the Gigosos & Cardeñoso model [45].

Digital photographs of TIAGO torch discharges were taken by a Canon EOS 2000D equipped with a SIGMA 105 mm lens (1/4000 s, f/10, ISO100) which allowed for the determination of both dart and plume lengths. Besides, a cathetometer with an uncertainty of 0.05 mm was utilized for dart length measuring and precise optical-fiber placement.

3. RESULTS AND DISCUSSION

3.1 Dart and Plume: morphology

As described previously [6,34], TIAGO microwave plasma source produces a torch-plasma structure with two distinguishable regions; a bright filament named dart which is surrounded by a less broad area called plume. To clearly identify those regions, photographs with several exposition times of plasmas under research were taken and are shown in Figure 3. For low exposure times, only the brighter zone (dart) is recorded in the images. However, increasing this parameter allows for registering the more tenuous shell (plume) that surrounds the dart and extends beyond it. In Table 1, the lengths of dart and plume are presented for each power condition. The dart length, from the nozzle exit to the start of the tenuous shell, was accurately measured using a cathetometer and verified with the photographs. As for the plume length, it was estimated from photographs taken with the longest exposure time (Figure 3) and considered from the end of the dart to the position at which no luminosity could be detected. For increasing powers, the dart becomes longer and the plume more voluminous as was also referred in [34]. The linear increase of the dart length with the applied power has also been reported for other torch-like devices at atmospheric pressure working with argon at 2.45 GHz [33,46]. In [46]

Hrycak et *al.* use powers higher than those presented in this research, while Snirer et *al.* [33] work with powers ranging from 10 to 300 W, so, in this research, a wide interval of powers is covered. Besides, dart length values are in good agreement to those previously reported [34], whereas plume ones are reported for the first time in this research.

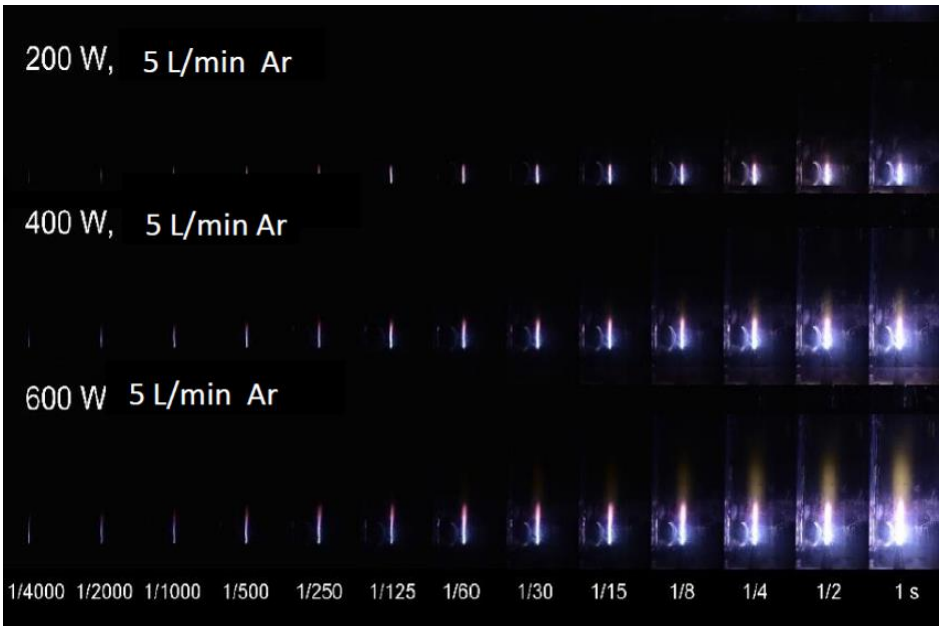

Figure 3: TIAGO plasma sustained using different powers photographed with increasing exposure times (in seconds).

Table 1: Dart and plume lengths for each power. Each length is an averaged value of several measurements.

Power (W)	Dart length (mm)	Plume length (mm)
200	5.7 ± 0.6	≈ 2
400	7.1 ± 0.4	≈ 6
600	8.8 ± 0.6	≈ 8.5

3.2 Gas temperature and electron density: different Zones along TIAGO torch plasma.

Gas temperature and electron density values are linked to the processes in which particles are involved; while electron density is a measure of the excitation and ionization capability of the discharge, gas temperature is a measure of the energy of heavy particles,

which is mainly acquired by elastic collisions with electrons. Both, electron density and gas temperature axial profiles are shown in Figure 4 for three different powers: 200, 400 and 600 W. For both parameters values, a similar trend is found regardless of the power.

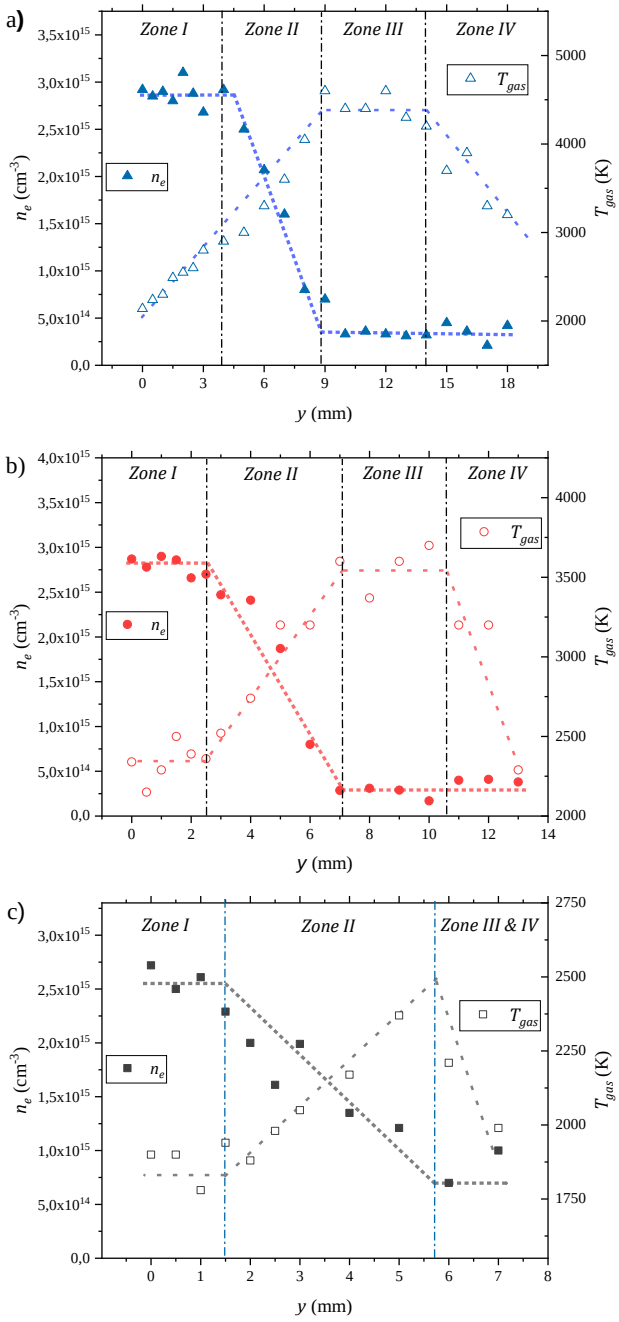

Figure 4. Discharge zones identification for a) 600 W, b) 400 W and c) 200 W. For each power, dart is constituted by *Zones I and II*. Uncertainty is always under 20 % for gas temperature and tends to be under 30% for electron density.

Concerning gas temperature, it increases along the dart and reaches a maximum at its end, decreasing from this position along the plume. This behavior matches with the

results found with other microwave plasma torches. It was observed in [47] for a TIA torch working with the same Ar flow (5.00 slm) and similar powers (700 W). Increasing the power supplied to the discharge leads to larger T_{gas}, more noticeable towards the end of the dart and in the plume region. In [31,48], Alves et *al.* obtained, feeding the discharge with the same argon flow, similar profiles of gas temperature in the TIA torch. However, sharper increase of gas temperature in the first millimeters from the nozzle is reported. Similar trend and values of this parameter are found in [49] by Leins et *al.* in a microwave-excited atmospheric plasma system based on an axially symmetric resonator. They use higher flows and powers, being the maximum 70 slm of Ar and 2 kW. Our results also fit with those shown in other microwave plasma torch-like devices. In [33], authors report an increase of gas temperature with both power and axial distance from the nozzle — specifically, gas temperature is shown to be higher in the middle of the dart than at the gas exit, which is also observed in the TIAGO dart—. Comparable values of gas temperature and an increase with applied power was also observed by Miotk et *al.* [50] at 915 MHz.

On the other hand, electron density remains almost constant under power changes in positions closest to the exit nozzle, except for the plasmas sustained at 200 W, where this plateau cannot be readily identified. From this preliminary zone, the density decreases linearly with similar slope until reaching a point where the number of electrons is small enough pointing out the end of the most energetic area of the plasma, *i.e.* the end of the dart, allowing to establish the limit between the dart and the plume of the TIAGO torch. Those values are in agreement with direct measurements of dart lengths as it is noted in Table 1. The values obtained are of the same order of magnitude than those shown by Garcia et *al.* in [43] with TIA discharge. The axial behavior is also similar to that found by Jonkers et *al.* in He [51,52] and Ar [52] TIA discharges as well as in [47] for an Ar/H_2 discharge by Ricard et *al.* also using TIA device. Moreover, Jonkers et *al.* [53] found this parameter to be always under $4 \cdot 10^{15}\ cm^{-3}$ in TIA discharges sustained by 1 kW microwave power coupled into an argon gas flow of 3.0 slm. An increase of electron density with power was also reported in [50], where values of the same order of magnitude are shown at 915 MHz. Furthermore, lineal decrease of electron density when moving far from the nozzle has been previously reported in other microwave plasma torches, as in [33] by Snirer et *al.* . However, the results reported herein allow for a more complete discussion regarding the behavior of the dart as a SWD.

From the analysis of the evolution of these parameters, some additional conclusions are drawn. Four Zones (or regions) can be identified along the axial direction of the torch when both T_{gas} and n_e are simultaneously plotted for each power condition. In the case of 600 W (Figure 4a) the plasma dart, which extends from 0 to 8.8 mm, appears constituted by two different regions (*Zones I* and *II*). In *Zone I*, which emerges just after the nozzle exit and lengthens for $3.5 - 4.0$ mm, the electron density remains almost constant. Next, in *Zone II* the electron density linearly decreases up to the end of the dart, contrary to the gas temperature behavior. Similarly, two regions can be also identified in the plume area; right after the end of the dart, (*Zone III*) both parameters maintain constant values being equal to that of the final position of the dart. Finally, in *Zone IV* which belongs to the end of the plume, gas temperature experiences a decrease while electron density keeps constant at a low value. Low non-zero electron density at some millimeters after the end of the discharge can be explained due to the presence there of a very low but non-negligible electromagnetic field. In [31], in the case of the TIA torch, it is theoretically shown that after the end of the dart the electromagnetic field sharply decreases but it does not reach a null value until some centimeters after the end of the discharge.

A similar analysis can be also carried out for discharges sustained at 400 and 200 W (Figures 4b and 4c). In Table 2 the length of the areas in each microwave power condition are presented. Those values are approximations obtained from *(i)* direct measurements, *(ii)* images taken from the plasma and *(iii)* the analysis of the plasma zones. It is worth noting that, as power decreases, the length of all zones is reduced. Particularly, for the smallest power condition (200 W); the reduction in the length of *Zones III* and *IV* is so significant that they cannot be truly differentiated from the plot in Figure 4c, which explains why both have been labeled together.

Table 2. Lengths of the different zones of the discharge.

Power (W)	**Dart length (mm)**		**Plume length (mm)**	
	Zone I	**Zone II**	**Zone III**	**Zone IV**
200	≈ 1.5	≈ 3.5	≈ 2.0	
400	≈ 2.5	≈ 4.5	≈ 3.5	≈ 2.5
600	≈ 3.8	≈ 5.0	≈ 4.5	≈ 4.0

3.3. Plasma kinetics: dart and plume.

To understand the processes taking place in the different regions of the dart and the plume, the radiation emitted was analyzed at different axial positions for each power considered. Figure 5 shows the radiation emitted by the plasma at different y—positions equal to 1.0, 5.0, 12.0 and 18.0 mm for 600 W, which correspond — according to Table 2 — to *Zones I*, *II*, *III* and *IV*, respectively. For ease of comparison, emission intensities were normalized to that of the 727.3 nm *Ar* line ($4p - 4s$) in *Zone I* since it is properly observed in every spectrum. Argon lines corresponding to $4p$, $5p$ and nd levels ($n = 5$, 6 and 7) can be identified in the spectra, as well as molecular bands owing to the interaction of the plasma with gases present in the air surrounding the discharge, such as nitrogen, oxygen and carbon dioxide, as it has been previously reported [32,34,53,54]. Both atomic and molecular species appear highlighted in Figure 5 for ease of identification, while Table 3 summarizes the observed molecular emissions.

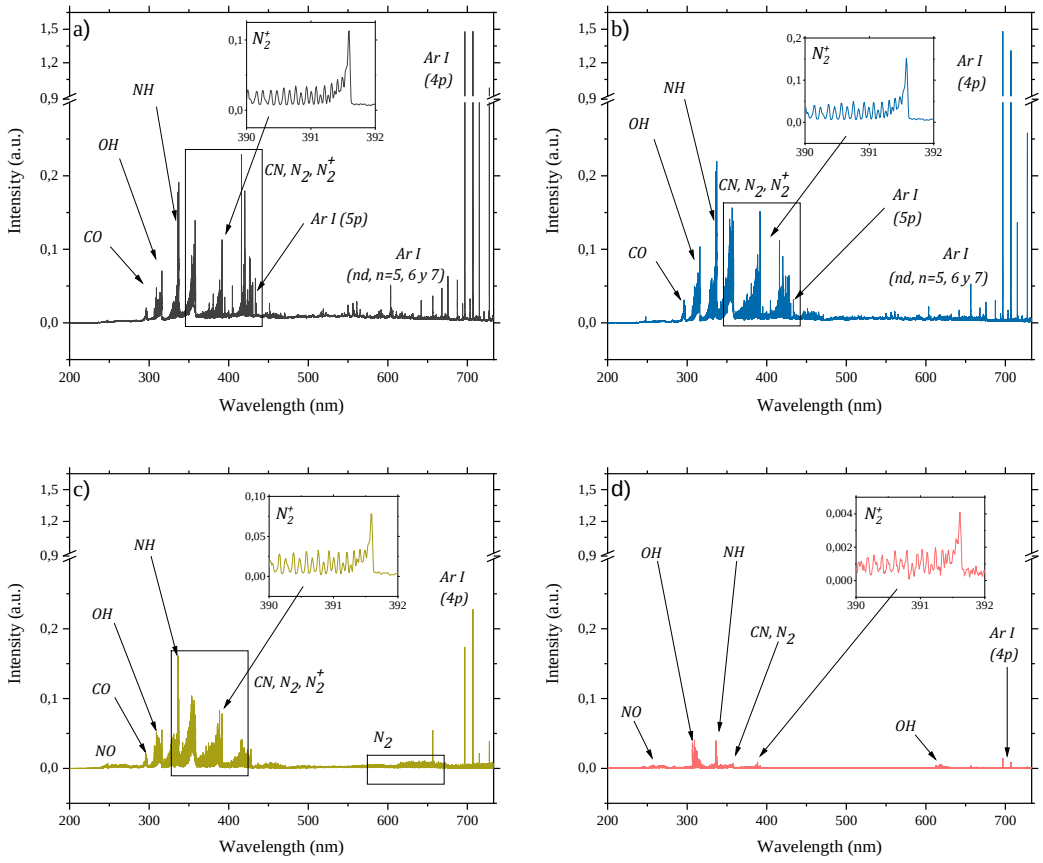

Figure 5: Emission spectra recorded at a) $y = 1.0$ mm, b) $y = 5.0$ mm, c) $y = 12.0$ mm and d) $y = 18.0$ mm of a 5.0 slm argon plasma sustained at 600 W. Spectra normalized to the intensity of 727.3 nm line recorded at $y = 1.0$ mm.

Table 3: Molecular species detected. Those in bold are the most intense transitions.

Molecule	System	Transition	Headbands (nm)
NO	γ	$A^2\Sigma^+ \rightarrow X^2\Pi$	247.1-247.9
$\boldsymbol{N_2}$	**Second positive**	$\boldsymbol{C^2\Pi_u \rightarrow B^3\Pi_g}$	**295.3, 296.2, 297.7, 313.6, 315.9, 337.1, 357.7, 405.9, 420.1**
	First positive	$B^3\Pi_g \rightarrow A^3\Sigma_u^+$	580.4, 654.5
$\boldsymbol{N_2^+}$	**First negative**	$\boldsymbol{B^2\Sigma_u^+ \rightarrow X^2\Sigma_g^+}$	**353.2, 354.9, 356.4, 358.2, 391.4, 423.7, 427.8**
$\boldsymbol{CN}$	**Cyanogen violet**	$\boldsymbol{B^3\Sigma \rightarrow X^2\Pi}$	**386.2, 387.1, 388.3, 460.4, 460.7, 460.9**
$\boldsymbol{NH}$	**3360 Å**	$\boldsymbol{A^3\Pi \rightarrow X^3\Sigma}$	**336.0**
CO	Third positive	$b^3\Sigma^+ \rightarrow a^3\Pi$	297.7

It is important to bear in mind that ionization processes control plasma kinetics at the beginning of the dart where electron density reaches its maximum whereas plasma becomes recombining along the dart as it was described in [32]. Therefore, modifications in plasma kinetics are expected along the different plasma zones. Indeed, as it is observed in Figure 5, for a given power, a progressive decrease of the intensity of atomic lines can be noticed for positions farther away from the nozzle; it is even more discernible for those originated upon deexcitation of the most energetic Ar levels ($5d$, $6d$ and $7d$) which tend to disappear. In contrast, the presence of molecular bands becomes more significant. In the farthest region, $y = 18.0$ mm, the emission spectrum is clearly dominated by molecular bands, mainly NO_γ, OH and NH species. Moreover, the nitrogen FNS (N_2^+) almost completely disappears in this region, as well as the argon lines belonging to the lowest detectable energy levels from argon ($4p$). These changes observed in the spectra clearly indicate modifications in the kinetics in different y—positions, supporting the existence of different zones. Nevertheless, as input power rises −for a fixed y—position− an increase in the intensities of the detected species is noticed, owing to the larger energy available for excitation processes, while the nature of those species is not modified. Therefore, plasma kinetics is not significantly altered as the power supplied to the discharge is increased.

Analyzing plasma spectra (Figure 5) together with T_{gas} and n_e axial profiles (Figure 4) and bearing in mind the identification of the different zones along the torch, some information on the kinetics of the particles existing in both dart and plume can be

extracted although the development of a kinetic model would eventually support the conclusions experimentally drawn. Furthermore, the following discussion is focused on the results for the plasma sustained at 600 W, where the different zones previously identified can be easily distinguished, although similar conclusions can be derived for the plasmas sustained with 200 and 400 W. For ease of understanding, general kinetics of Ar plasmas with entrance of O_2 and N_2 at atmospheric pressure are going to be hereunder indicated.

As it is known, in atmospheric-pressure microwave plasmas, excitation and ionization of Ar atoms are carried out step-wise by collisions with electrons, being the $4s$ metastable levels (Ar^m) the departure level for the excitation and ionization processes (reactions 1 and 2) [52,55], requiring high-energy electrons (> 11.5 eV, see Figure 6) from the tail of the EEDF (electron energy distribution function) for its generation. However, in TIAGO torch discharge this kinetics is highly influenced by the interaction of the argon-based plasma with the surrounding atmosphere, especially nitrogen, through reactions (3) and (4). Air presence is responsible for the appearance of molecular ions and excited molecular species, mainly with nitrogen content, including N_2^+ and N_2^*. The formation of these species has been previously studied and reported in this torch-like plasmas [34]; charge transfer (3) and Penning excitation (4) reactions were ascribed to the formation of $N_2^+\left(X^2\Sigma_g^+\right)$ molecular ions and of excited $N_2(C^3\Pi_u)$ molecules due to resonant energy of the corresponding ionic (15.8 eV for Ar^+ and 15.6 eV for $N_2^+\left(X^2\Sigma_g^+\right)$ [56]) and excited (11.7 eV for $Ar(4s)$ and 11.1 eV for $N_2(C^3\Pi_u)$) species, respectively [57] (Figure 6).

$$Ar + e^- \longrightarrow Ar^m + e^- \quad (1)$$

$$Ar^m + e^- \longrightarrow Ar^* + e^- \quad (2)$$

$$Ar^+ + N_2\left(X^1\Sigma_g^+\right) \longrightarrow Ar^0 + N_2^+\left(X^2\Sigma_g^+\right) \quad (3)$$

$$Ar^m + N_2\left(X^1\Sigma_g^+\right) \longrightarrow Ar^0 + N_2(C^3\Pi_u) \quad (4)$$

The detection of the first negative system (FNS, $B^2\Sigma_u^+ \rightarrow X^2\Sigma_g^+$) requires prior excitation of the $N_2^+\left(X^2\Sigma_g^+\right)$ ground level of these molecular ions to the $N_2^+(B^2\Sigma_u^+)$ excited state, which can mainly happen through inelastic collisions with electrons of

energies ≥ 2.5 eV and belonging to the bulk of the electron energy distribution function (EEDF), following reaction (5) [58].

$$N_2^+\left(X^2\Sigma_g^+\right) + e^- \longrightarrow N_2^+(B^2\Sigma_u^+) + e^- \quad (5)$$

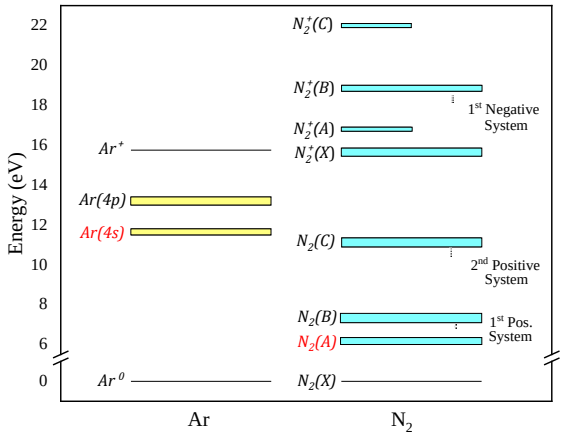

Figure 6. Main energy levels of the Ar atom and N_2 molecule. Metastable levels are labeled in red.

Other molecular bands are also observed in the spectra of the TIAGO dart due to the deexcitation of $N_2(C^3\Pi_u)$, giving place to the second positive system (SPS, $C^2\Pi_u \rightarrow B^3\Pi_g$), which leads to the population of $N_2\left(B^3\Pi_g\right)$ and the formation of $N_2(A^3\Sigma_u^+)$ through the emission of the first positive system (FPS, $B^3\Pi_g \rightarrow A^3\Sigma_u^+$) (Figure 6). Nonetheless, according to [59,60] the upper level $N_2\left(B^3\Pi_g\right)$ can be reached by the recombination of $N-$ atoms in the gas volume of a $Ar-N_2$ afterglow by reaction (6) giving then place to the emission of the FPS. Actually, the emission of the FPS has been pointed out as a fingerprint of nitrogen atoms in the plasma afterglow [60].

$$N + N + N_2 \longrightarrow N_2(B) + N_2 \quad (6)$$

According to [60-63] at microwave discharges operated at atmospheric pressure, high dissociation rates of N_2 into atomic nitrogen (7) and O_2 into atomic oxygen (8) by electron collisions can be obtained even with low percentage concentrations of these gases. Besides, according to [56] nitrogen atoms with high kinetic energy can also be formed by dissociative recombination of N_2^+ ions (9) [63,64]. Therefore, the presence of N and O atoms is likely in TIAGO torch discharges, although OI and NI atomic emissions are not observed in the spectra since their most intense emissions are out of the wavelength range recorded.

$$N_2(X) + e^- \longrightarrow N\left(^4S\right) + N\left(^4S\right) + e^- \quad (7)$$

$$O_2(X) + e^- \longrightarrow O\left(^3P\right) + O\left(^3P\right) + e^- \quad (8)$$

$$N_2^+(X) + e^- \longrightarrow N\left(^4S\right) + N\left(^4S\right) \quad (9)$$

The existence of both nitrogen and oxygen atoms can explain the emission of NO_γ band due to the deexcitation of NO molecules from $A^2\Sigma^+$excited state to the $X^2\Pi$ ground state. According to [65] the excitation of $NO(A^2\Sigma^+)$ can be reached following equations (10) and (11), being M a third body such as Ar atoms or other heavy species, after having obtained the ground state level of NO molecules by either reactions of N atoms with O_2 molecules (12) or collisions of excited nitrogen ($A^2\Sigma^+$) with $O-$ atoms (13) [66]. Nevertheless, for the T_{gas} range found under the experimental conditions of this research, the coefficient rates of equations (10) and (12) are higher as compared to those of (11) and (13) [66], being therefore more likely and thus responsible for the emission of NO_γ band.

$$NO(X) + N_2(A^3\Sigma_u^+) \longrightarrow NO(A^2\Sigma^+) + N_2(X) \quad (10)$$

$$N\left(^4S\right) + O\left(^3P\right) + M \longrightarrow NO(A^2\Sigma^+) + M \quad (11)$$

$$O_2 + N\left(^4S\right) \longrightarrow NO(X) + O\left(^3P\right) \quad (12)$$

$$N_2(A^3\Sigma_u^+) + O\left(^3P\right) \longrightarrow NO(X) + N\left(^2D\right) \quad (13)$$

Finally, high-energy nitrogen atoms from reaction (9) can produce excited excimers together with the dissociation products of molecules in air ambience, *i.e.* CO_2, allowing for the formation of CN excited states by three body recombination (14), being M a third body.

$$C + N + M \longrightarrow CN(B^2\Sigma) + M \quad (14)$$

In Figure 7 is possible to observe the profile of the intensity of the N_2^+ (391.4 nm FNS), CN (388.3 nm, Cyanogen system) and N_2 (357.7 nm, SPS) band heads along the $y-$axis together with the dart length. Focusing on the FNS (Figure 7a), right after the nozzle, N_2^+ intensity is constant until $y \sim 2$ mm, and then increases, reaching a maximum slightly before the end of the dart to later decrease along the plume until disappearing at its end. As power is increased, larger values of N_2^+ intensities are registered owing to the

larger energy available in the discharge, as previously stated. As compared to N_2^+ (391.4 nm FNS), the intensity profile of CN (388.3 nm) follows a similar trend. The constant behavior of its intensity along *Zone I* might be explained by a limited interaction of air with the dart along this region since $C-$ atoms can only be obtained from air constituents. This assumption coincides with low air fraction in argon due to diffusion modelled in an atmospheric pressure argon plasma jet in air [67]. Concerning the intensity of the SPS, it behaves similarly as the intensity of FNS except along *Zone I* where it decreases reaching a local minimum at the end of this region ($y \sim 2$ mm).

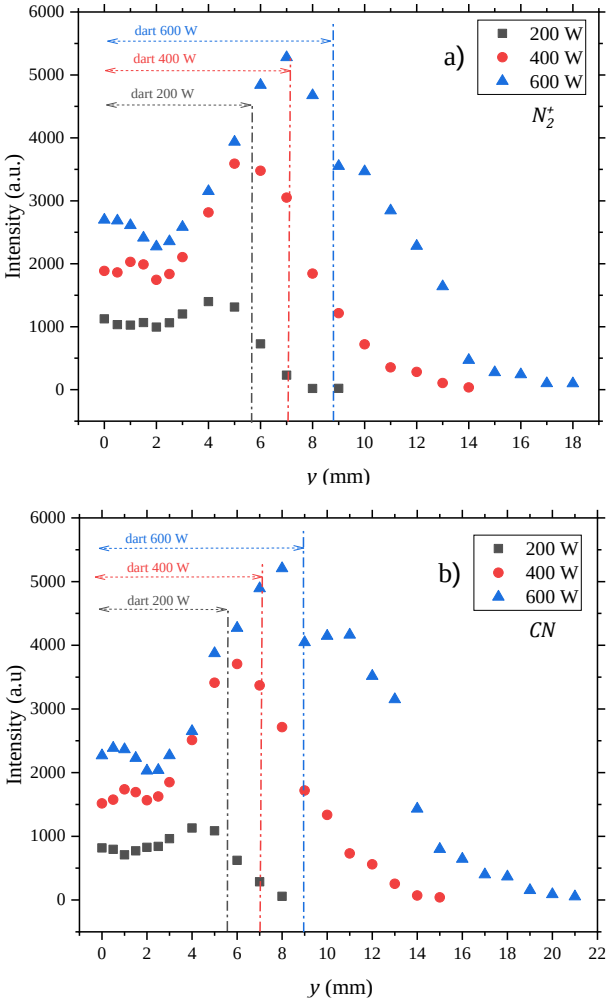

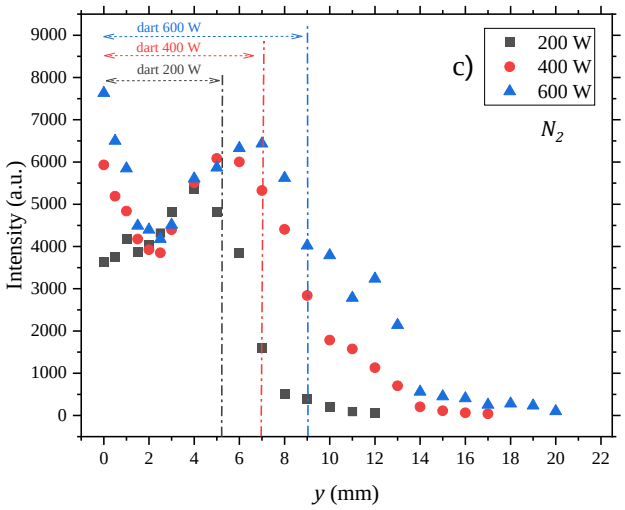

Figure 7. N_2^+ (391.4 nm FNS), CN (388.3 nm, Cyanogen system) and N_2 (357.7 nm, SPS) band head intensity along the $y-$axis

Moving to studying atomic species, a significant number of Ar spectral lines can be identified in the recorded spectra (Figure 5), whereas N or O spectral lines could not be detected within the wavelength range recorded. Since the intensity of a spectral line is proportional to the population density of the upper level of the associated transition, in Figure 8 the intensity of Ar atomic emitted at 714.7 ($4p \longrightarrow 4s$), 430.0 ($5p \longrightarrow 4s$) and 560.6 ($5d \longrightarrow 4p$) nm appears depicted for each power condition as representative of their transition (lines of a same transition show a similar behavior).

As it can be observed in Figure 8, the intensity of ArI lines decreases, which is specially noticeable in *Zone I* for line 714.7 nm regardless of the applied power. The intensity of this line is proportional to the population of the $Ar(4p)$ level, which is mainly populated via inelastic collisions with electrons from the $Ar(4s)$ level reaction (2), being therefore both closely related (see Figure 6). Consequently, the depopulation of $4p$ levels can be interpreted as a reduction in the number of the lowest argon excited states, *i.e.* metastable argon atoms, which are also involved in the formation of excited nitrogen molecules such as $N_2(C^3\Pi_u)$ according to reaction (4). Nevertheless, the decrease in the intensity of the SPS (see Figure 7c) suggests that either Ar^m metastable density or nitrogen molecules along *Zone I* are being decreased. Assuming that nitrogen entrance is constant along the aforementioned region according to the constant behavior of CN intensity, the decrease of the SPS must be due to a reduction of metastable states of $Ar-$ atoms. Therefore, as $Ar(4p)$ and $N_2(C^3\Pi_u)$ excited states population depends on

metastable states and both decrease in *Zone I*, the loss of Ar^m excited atoms could be assumed and ascribed to their pooling (see reaction 15) in this region.

$$Ar^m + Ar^m \longrightarrow Ar^+ + Ar^0 + e^- \quad (15)$$

Through reaction (15), e^- and Ar^+ are formed which should be related to an increase in electron density as well as the emission of the FNS by the formation of N_2^+ through charge transfer reaction (3) as its departure point (5). However, both electron density and the emission of FNS along *Zone I* remains constant as it is shown in Figures 4 and 7a, respectively. Therefore, another process must be involved in this region kinetics. It is worth also remarking that in *Zone I*, T_{gas} tends to increase (Figure 4), more noticeably in discharges sustained at 600 W. According to Moon and Choe [56] who studied the effects of air ambience in Ar −based discharges working at atmospheric pressure, the N_2^+ ion can be destroyed through reaction (9) giving place to nitrogen atoms which provide energy to increase T_{gas} (assumed to be equal to T_{rot}) since they have a relatively high kinetic energy via exothermic dissociative recombination reactions. Hence, this process could explain the constancy in *Zone I* of n_e and the emission of the FNS and the increase in T_{gas} in this region as well.

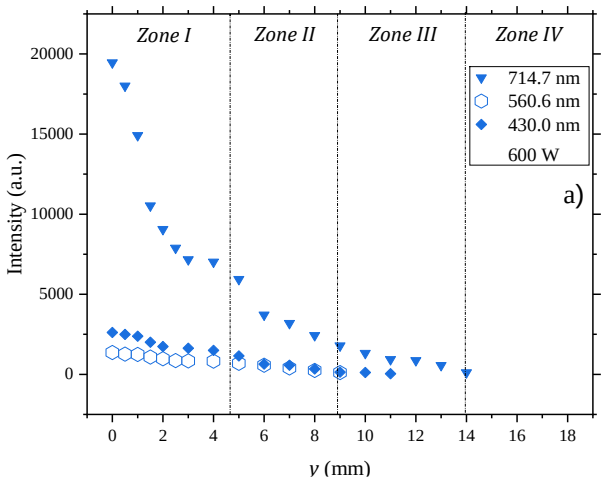

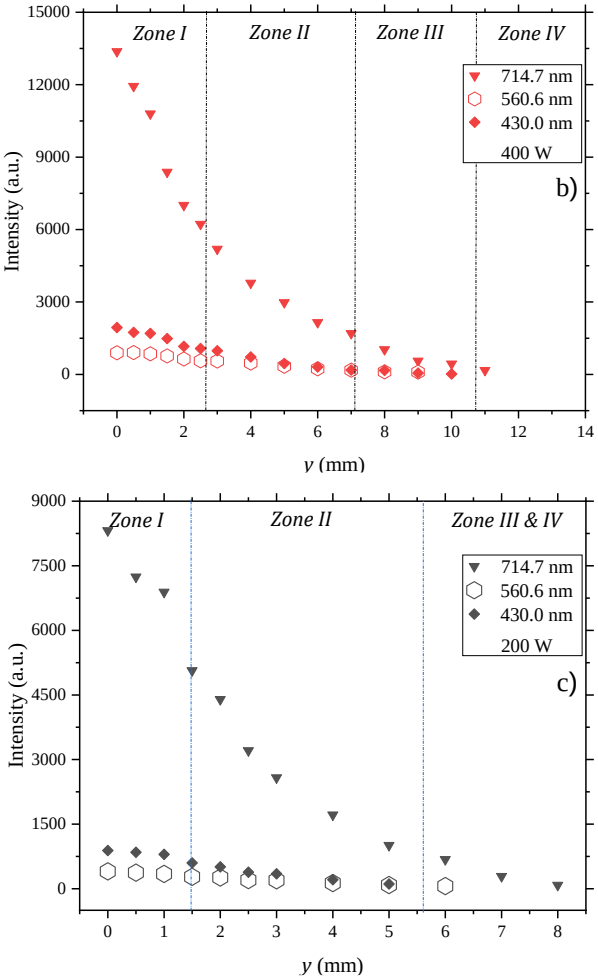

Figure 8. Intensity of selected *Ar I* lines along the discharge axis for plasmas sustained at a) 600 W, b) 400 W and c) 200 W.

In *Zone II*, a better mixing of the surrounding air with the argon flow is achieved as is noticed in the increase in the emission of $CN(B^2\Sigma)$, $N_2^+(B^2\Sigma_u^+)$ and $N_2(C^3\Pi_u)$ (Figure 7) while Ar excited states are being depopulated (Figure 8). This experimental result gives place to two scenarios. On the one hand, a partial depletion of the EEDF tail can take place by collisions of fast electrons with nitrogen molecules in the ground state, thus creating excited levels of N_2 molecules. This would also lead to a lower population of Ar^m and the perturbation of excitation/ionization chain of $Ar-$ atoms, resulting in a decreasing number of electrons. On the other hand, a larger N_2 concentration in the gas would result in a more important competition between $Ar-$ atoms and N_2- molecules for low energy electrons belonging to the bulk of the EEDF, resulting in an enhancement of reactions leading to the generation of $N_2(C^3\Pi_u)$ and $N_2^+(B^2\Sigma_u^+)$ instead of argon ions or excited states. Thus, the intensity of atomic Ar lines decreases along this zone following the behaviour of electron density, but also influenced by the interactions with

nitrogen species. Interestingly, according to Figure 7a, the intensity of the FNS in *Zone II* increases reaching a maximum slightly before the end of the dart while T_{gas} reaches its maximum at the end of the dart and then tend to be constant. This behaviour can be explained by the destruction of nitrogen ions detailed previously through reaction (9) providing this region with a higher density of $N-$ atoms. Indeed, the emission of the FPS, $N_2(B^3\Pi_g \rightarrow A^3\Sigma_u^+)$ started being detectable in positions where FNS reaches its maximum tending to be more noticeable as FNS intensity decreases which supports the idea of the destruction of N_2^+ in the latter positions of Zone II by (9) since nitrogen atoms are required for the emission of the FPS [59,60].

The kinetics in the plume region dramatically change; the density of charged particles, *i.e.* electrons and positive ions, tends to reduce regardless of the input power and emitted spectra show mainly molecular emissions. Indeed, the fact that metastable nitrogen excited species ($N_2(A^3\Sigma_u^+)$) are detected in the plume region (mainly in *Zone III*) (Figure 5c) together with the emission of NO_γ band (Figure 5c, 5d) with the reduced presence of charged particles suggests that the plume could behave as an afterglow (postdischarge) observed after N_2-O_2 −based discharges as it has been extensively reported [59-65] although the non-negligible concentration of charged particles needs to be discussed.

As it is observed in Figure 4a, electron density presents a non-negligible concentration in the *Zone III* and keeps an almost constant value from the dart end along the plume. According to [68], the EEDF is largely modified at the earlier positions of the postdischarge, and its high-energy tail is rapidly depopulated due to inelastic electron collisions, making thus excitation or ionization highly improbable. However, these low-energy electrons can contribute to the excitation of rotational and vibrational states, allowing to keep the gas temperature at a constant value (Figure 4). Ionization in this zone is still possible through collisions between long-lived metastable $N_2(A^3\Sigma_u^+)$ molecules (16), resulting in vibrationally excited neutral nitrogen molecules and the generation of low energy electrons ($0-1.3$ eV), thus partly compensating the loss of electrons by recombination with $Ar-$ and N_2- ions.

$$N_2(A^3\Sigma_u^+) + N_2(A^3\Sigma_u^+) \longrightarrow N_2\left(X^1\Sigma_g^+\right) + N_2^+\left(X^2\Sigma_g^+\right) + e^- \qquad (16)$$

Besides, the torch plume is also in contact with the air contained in the reactor, as it can be observed by the enlarging of the plume region (Figure 3). The decrease of the

$N_2^+(B^2\Sigma_u^+)$ intensity (Figure 7) owes to a decrease in its formation by electron impact from $N_2^+\left(X^2\Sigma_g^+\right)$ due to the depletion of the EEDF in the postdischarge, but these species can still be formed from existing nitrogen molecular ions in the ground level by reaction (17).

$$N_2\left(X^1\Sigma_g^+, v\right) + N_2^+\left(X^2\Sigma_g^+\right) \longrightarrow N_2\left(X^1\Sigma_g^+, v = 0\right) + N_2^+(B^2\Sigma_u^+) \quad (17)$$

Reactions (16) and (17) might contribute to the loss of long-lived excited nitrogen species along the postdischarge up to positions in *Zone IV*, where only neutral species can be detected (Figure 5d), whose excitation can be attributed to collisions of these species with the remaining metastable and vibrationally excited particles arriving to this zone carried by the gas flow.

3.4. Dart as a surface wave discharge

Based on the well-established literature concerning SWDs sustained at atmospheric pressure [55], their main characteristics are: *(i)* the increment of plasma length with the power supplied to the discharge, *(ii)* the linear decreasing of electron density along the discharge axis, and *(iii)* the invariance of the electron density at a given axial distance *z* measured from the end of the plasma column. Recently, Moisan and Nowakowska [6] have included another feature for SWDs, that is the existence of a plasma segment of some millimeters, which extends right after the power launcher, being this segment an essential part where ionization and recombination processes are balanced, thus leading to a relative maximum of electron density. This segment is considered a non-SWD plasma segment, previous to the establishment of the surface wave, where some microwave power is radiated through non-guided (space-wave) radiation, being more noticeable for higher applied powers. Consequently, strictly speaking, the SWD does not start immediately after the wave-launcher exit, but some distance after it.

Figure 9 shows the axial profiles of electron density from Figure 4 plotted against the $z-$position, measured from the end of the plasma dart, as shown in Figure 2, considering $z = 0$ the end of the dart. These results agree well with the description of a SW plasma within the uncertainty of the measurements, thus showing its invariance respect the position measured from the end of the column. Moreover, the slope of all the

electron density profiles is nearly the same, which is also a distinctive feature of surface wave discharges for a given gas composition and vessel dimensions.

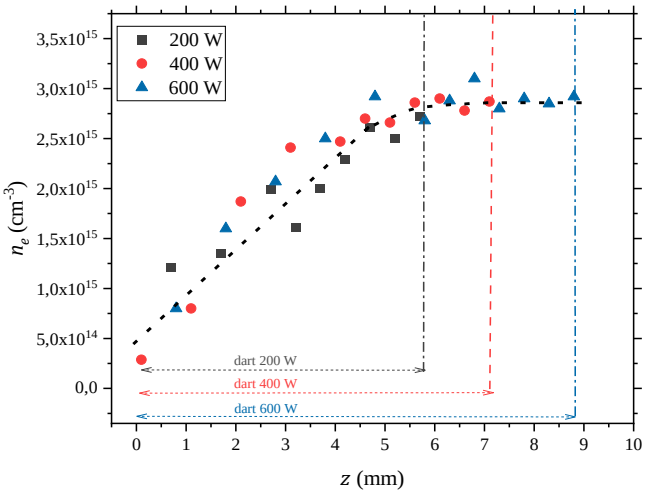

Figure 9. Electron density along the discharge axis measured from the end of the plasma column ($z = 0$). The uncertainty tends to be under 30 %.

What has been previously identified as *Zone I* in our discharges matches with the description of the radiation zone theoretically predicted in [6]: a non-SWD zone whose length increases with the power supplied to the discharge (Table 2) where electron density maintains an almost constant value (Figure 4). Besides, according to numerical analysis of Nowakowska et *al*. for TIAGO torch discharges [69], and under the experimental conditions of our research, the unshielding of this plasma source results in the radiation of electromagnetic energy into space, especially along positions closer to the nozzle exit, *i.e. Zone I*, which is estimated to be around 43%. Also, in [70] it can be found evidence supporting the existence of the radiation zone in a microwave plasma torch, although in that research it was neither mentioned nor identified. So, it is the first time the existence of radiation zone at atmospheric pressure has been experimentally reported in a microwave plasma torch. As for *Zone II*, the linear decrease of the electron density with a similar slope for all considered powers and its invariance respect to the end of the discharge (Figure 9) matches the expected behavior of a SWD together with an increase of length with the microwave power (Table 2).

The intensity of the Ar atomic lines considered in the current study appears also depicted as function of $z-$position (Figure 10). The intensity of ArI lines (560.0 and 430.0 nm) is linear with z, similarly as n_e (Figure 9), with increased intensities for larger input powers supplied to the discharge. These results agree well with those reported for

SWDs using a surfatron as excitation device [71], owing to the fact that these levels ($5p$ and $5d$) are mainly populated step-wise by inelastic collisions of excited argon atoms $-Ar(4p)$ levels$-$, with electrons belonging to the bulk of the EEDF ($<$ 2 eV). However, the intensity of the 714.7 nm$-$ $Ar(4p)$ does not show the same linear decrease towards the end of the dart. As it has been discussed before, the population of these levels ($4p$) is closely related to that of the metastable levels, being populated in pure argon discharges by inelastic collisions of electrons with metastable levels (2). Under the experimental conditions of this research, nitrogen entrance in the dart from the surrounding air strongly modifies the population of metastable levels due to both Penning excitation of nitrogen molecules (4), leading to a decrease in the density of argon metastable atoms that propagates to $4p$ levels, which cease following the trend of the electron density. According to [72], modifications in ($4s$) levels of Ar propagates more readily to ($4p$) levels. The intensity of FNS system of N_2^+ in $z-$positions is depicted in Figure 10d. As it has previously discussed, intensity of these emissions is constant in close to the nozzle positions (Figure 7a) and then increases until reaching a maximum slightly before the end of the dart. When plotting in $z-$system, this maximum is observed to appear in the same $z-$position ($z = 1.9 \pm 0.2$ mm) regardless the input power. It derives from the fact that reaction (9), which governs the decrease of FNS intensity, is mediated by electrons, and electron density has been found to have no dependency on the input power in $z-$system (Figure 9).

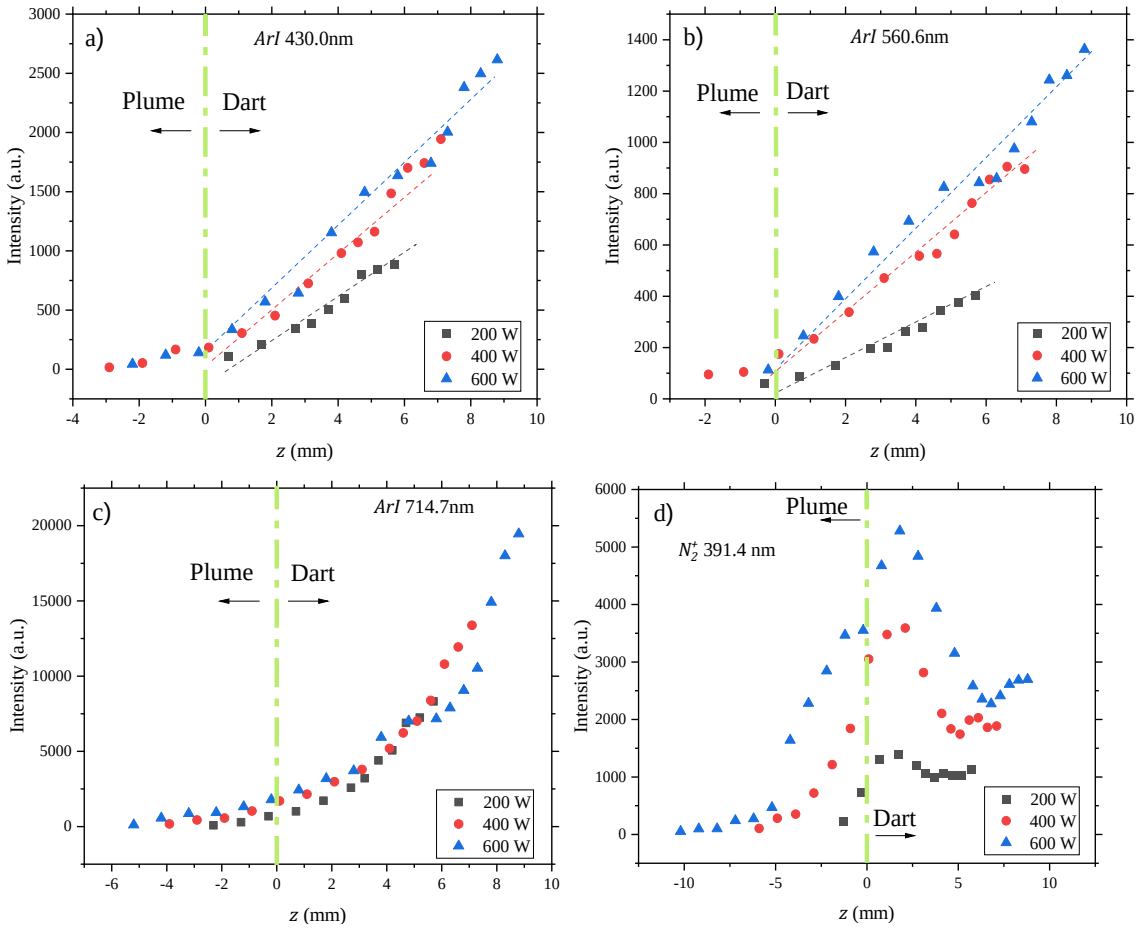

Figure 10. Intensity of selected *Ar I* lines a) 430.0 nm, b) 560.6 nm, c) 714.7 nm and d) the N_2^+ (391.4 nm FNS), along the discharge axis.

These results are similar to those experimentally found and reported for SWDs [71,73], allowing to identify the dart of a TIAGO torch as a surface wave discharge as it was theoretically predicted by Moisan et *al.* [6] and partially supported by Alves modelling [31]. However, for this to happen, surrounding air should act as virtual cylindrical dielectric vessel enabling the existence between plasma and atmosphere of an interface through which electromagnetic surface wave could propagate. Conditions of air to be a proper dielectric are stated in [23]. There, Nowakowska et *al.* examined the characteristics of electromagnetic waves propagating along dense plasma filaments at atmospheric pressure. Moreover, the ambience surrounding the plasma must be composed of a gas or mixture of gases having a higher ionization potential than that of the plasma carrier gas.

As discussed in [24], in the experimental conditions of flow of this work, the discharge is more efficiently shielded from the surrounding atmosphere than in the case

of low Ar flows. However, the presence of air surrounding the discharge is essential as it allows the surface wave to propagate along the discharge. This feature can be observed in Figure 11 where TIAGO torch discharge pictures are taken when the discharge is generated within air, i.e. the experimental conditions of this research, (Figure 11a) and pure argon (Figure 11b) atmospheres. When the plasma is generated inside the reactor filled with argon, the single filament structure observed in air-surrounding discharge disappears because there is not an effective interface between plasma and atmosphere and, so, the virtual dielectric cylinder does not exist to enable the propagation of the wave. Therefore, chaotic filamentation takes place and the plasma extinguished in few seconds. Consequently, no reliable spectroscopic measurements can be performed. However, when the discharge is surrounded by ambient air, with an ionization potential higher than that of the carrier gas, acts as a dielectric cylinder enclosing the discharge allowing for a stable configuration of the plasma similar to that of a SWD. A rough percentage estimation of air components sampled in the upper part of the reactor atmosphere was carried out by means of mass spectrometry, following the same procedure described in [35]. In pure argon environment (Figure 11b) the amount of nitrogen and oxygen remains below 0.5% of the total flow gas whereas it increases ca. 100 times when the discharge is generated within air (Figure 11a) which supports the previous discussion.

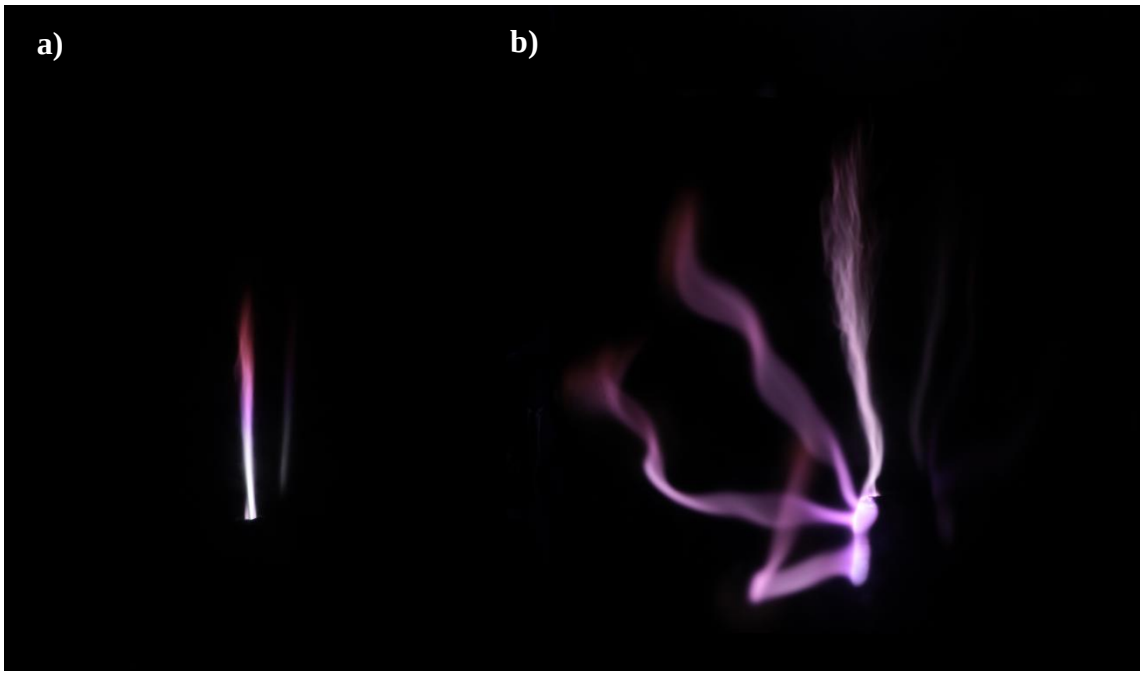

Figure 11. TIAGO plasma photographs generated at 400 W in an atmosphere of a) ambient air (1/4000 s) b) argon gas (1/640 s).

Conclusions

In this experimental research, TIAGO torch discharges at different powers have been created and characterized by means of Optical Emission Spectroscopy technique. The morphology of the plasma has been studied by using both a cathetometer and photographs analysis and two different regions, the dart and the plume, can be clearly identified. When increasing applied power, the dart becomes longer and the volume of the plume noticeably increases.

When considering the axial profile of the main plasma parameters –gas temperature and electron density– different zones can be identified inside both the dart and the plume. Gas temperature increases along the dart (*Zones I* and *II*), then reaches a plateau (*Zone III*) and then decreases (*Zone IV*). Electron density remains almost constant in positions closest to the nozzle *(Zone I*) and then decreases linearly with similar slope until the end of the dart (*Zone II*) while in the plume, the number of electrons remains quite low (*Zones III* and *IV*). The length of each zone, as well as its reduction with the increase of the applied power, has been reported. Moreover, gas temperature has been found to increase with power, contrarily to what happens in the case of electron density.

Once characterized the axial profiles of the main plasma parameters, atomic and molecular emissions are recorded and depicted so variations in internal kinetics along the different Zones identified in discharge and postdischarge have been discussed taking into account the influence of gas entrance from the surrounding atmosphere.

Finally, the behavior of the dart as a surface wave discharge has been verified. *Zone I* has been found, first-ever supported by experimental measurements, to be a radiation zone previous to the establishment of the surface wave in *Zone II.* It can be proven through the study of the axial profile of electron density, which matches the expected behavior of a surface wave discharge. The increase of dart length with the microwave power is another distinguishing feature of this kind of plasmas.

The work here presented, despite being in agreement with models showing SWD features, is circumscribed to the spectroscopic characterization of the discharge. A further theoretical approach by modelling would complement the results herein presented. The development of a numerical model encompassing plasma kinetics, fluid dynamics, and electromagnetic field simulation would help visualizing both the field distribution and the discharge structure fitting the SWD-like arrangement. However, these results are a

valuable contribution to the understanding of the internal performance of Surface Wave Discharges and constitute a step towards the optimization of the technological applications of the TIAGO torch discharges in many fields such as graphene production or green hydrogen generation and the possible development of new applications.

Declaration of Competing Interest

The authors declare that they have no known competing financial interests or personal relationships that could have appeared to influence the work reported in this paper.

Data availability

Data will be made available on request.

Acknowledgements

Information avoided to favor the anonymizing process.

References

[1] Tuma, D. T. (1970). A quiet uniform microwave gas discharge for lasers. Review of Scientific Instruments, 41(10), 1519-1520. https://doi.org/10.1063/1.1684334

[2] Dias, A., Bundaleska, N., Felizardo, E., Tsyganov, D., Almeida, A., Ferraria, A. M., ... & Tatarova, E. (2022). N-Graphene-Metal-Oxide (Sulfide) hybrid Nanostructures: Single-step plasma-enabled approach for energy storage applications. Chemical Engineering Journal, 430, 133153. https://doi.org/10.1016/j.cej.2021.133153

[3] Muñoz, J., Bravo, J. A., & Calzada, M. D. (2017). Aluminum metal surface cleaning and activation by atmospheric-pressure remote plasma. Applied Surface Science, 407, 72-81. https://doi.org/10.1016/j.apsusc.2017.02.092

[4] Bigras, G. R., Glad, X., Martel, R., Sarkissian, A., & Stafford, L. (2018). Treatment of graphene films in the early and late afterglows of N2 plasmas: comparison of the defect generation and N-incorporation dynamics. Plasma Sources Science and Technology, 27(12), 124004. https://doi.org/10.1088/1361-6595/aaedfd

[5] Rincón, R., Muñoz, J., Morales-Calero, F. J., Orejas, J., & Calzada, M. D. (2021). Assessment of two atmospheric-pressure microwave plasma sources for H2 production

from ethanol decomposition. Applied Energy, 294, 116948. https://doi.org/10.1016/j.apenergy.2021.116948

[6] Moisan, M., & Nowakowska, H. (2018). Contribution of surface-wave (SW) sustained plasma columns to the modeling of RF and microwave discharges with new insight into some of their features. A survey of other types of SW discharges. Plasma Sources Science and Technology, 27(7), 073001. https://doi.org/10.1088/1361-6595/aac528

[7] Nowakowska, H., Lackowski, M., & Moisan, M. (2020). Radiation Losses from a Microwave Surface-Wave Sustained Plasma Source (Surfatron). IEEE Transactions on Plasma Science, 48(6), 2106-2114. https://doi.org/10.1109/TPS.2020.2995475

[8] Rachdi, L., Sushkov, V., & Hofmann, M. (2022). Optical emission spectroscopy diagnostics for plasma parameters investigation in a Duo-Plasmaline surface-wave sustained discharge. Spectrochimica Acta Part B: Atomic Spectroscopy, 106432. https://doi.org/10.1016/j.sab.2022.106432

[9] Dorbin, M. R., Mohassel, J. A. R., Sadeghikia, F., & Ja'afar, H. B. (2022). Analytical Estimation of the Efficiency of Surface-Wave-Excited Plasma Monopole Antennas. IEEE Transactions on Antennas and Propagation, 70(4), 3040-3045. https://doi.org/10.1109/TAP.2021.3139967

[10] Moisan, M., & Zakrzewski, Z. (1991). Plasma sources based on the propagation of electromagnetic surface waves. Journal of Physics D: Applied Physics, 24(7), 1025. https://doi.org/10.1088/0022-3727/24/7/001

[11] Moisan, M., P. Leprince, C. Beaudry, E. Bloyet, Improvements relating to devices and methods of using HF waves to energize a column of gases enclosed in an insulating casing, US patent 4,049,940 1977.

[12] Glaude, V. M. M., Moisan, M., Pantel, R., Leprince, P., & Marec, J. (1980). Axial electron density and wave power distributions along a plasma column sustained by the propagation of a surface microwave. Journal of Applied Physics, 51(11), 5693-5698. https://doi.org/10.1063/1.327568

[13] Tendero, C., Tixier, C., Tristant, P., Desmaison, J., & Leprince, P. (2006). Atmospheric pressure plasmas: A review. Spectrochimica Acta Part B: Atomic Spectroscopy, 61(1), 2-30. https://doi.org/10.1016/j.sab.2005.10.003

[14] Jimenez, M., Rincon, R., Marinas, A., & Calzada, M. D. (2013). Hydrogen production from ethanol decomposition by a microwave plasma: Influence of the plasma gas flow. International journal of hydrogen energy, 38(21), 8708-8719. https://doi.org/10.1016/j.ijhydene.2013.05.004

[15] Marec, J. & Leprince, P. (1993). Microwave discharges fundamentals and applications, Ed. C.M. Ferreira and M. Moisan, Plenum: New York, 45

[16] Beenakker, C. I. M. (1976). A cavity for microwave-induced plasmas operated in helium and argon at atmospheric pressure. Spectrochimica Acta Part B: Atomic Spectroscopy, 31(8-9), 483-486. https://doi.org/10.1016/0584-8547(76)80047-X

[17] Choi, J., Iza, F., Do, H. J., Lee, J. K., & Cho, M. H. (2009). Microwave-excited atmospheric-pressure microplasmas based on a coaxial transmission line resonator. Plasma Sources Science and Technology, 18(2), 025029. https://doi.org/10.1088/0963-0252/18/2/025029

[18] M. Moisan, P. Leprince, C. Beaudry and E. Bloyet, Perfectionnements apportées aux dispositive d'excitation par des ondes HF d'une colonne de gaz enfermée dans un envelope, Brevet, France (1974).

[19] M. Moisan, R. Etemadi and J.C. Rosating, French Patent No. 2 762 748, European Patent N0 EP 0 874 537 A1

[20] Moisan, M., Chaker, M., Zakrzewski, Z., & Paraszczak, J. (1987). The waveguide surfatron: a high power surface-wave launcher to sustain large-diameter dense plasma columns. Journal of Physics E: Scientific Instruments, 20(11), 1356. https://doi.org/10.1088/0022-3735/20/11/009

[21] Camuna-Aguilar, J. F., Pereiro-Garcia, R., Sanchez-Uria, J. E., & Sanz-Medel, A. (1994). A comparative study of three microwave-induced plasma sources for atomic emission spectrometry-II. Evaluation of their atomization/excitation capabilities for chlorinated hydrocarbons. Spectrochimica Acta Part B: Atomic Spectroscopy, 49(6), 545-554. https://doi.org/10.1016/0584-8547(94)80047-2

[22] Moisan, M., Zakrzewski, Z., & Rostaing, J. C. (2001). Waveguide-based single and multiple nozzle plasma torches: the TIAGO concept. Plasma Sources Science and Technology, 10(3), 387. https://doi.org/10.1088/0963-0252/10/3/301

[23] Moisan, M., Sauve, G., Zakrzewski, Z., & Hubert, J. (1994). An atmospheric pressure waveguide-fed microwave plasma torch: the TIA design. Plasma Sources Science and Technology, 3(4), 584. https://doi.org/10.1088/0963-0252/3/4/016

[24] Margot, J., & Moisan, M. (1993). Characteristics of surface-wave propagation in dissipative cylindrical plasma columns. Journal of plasma physics, 49(3), 357-374. https://doi.org/10.1017/S0022377800017062

[25] Grosse, S., Georgieva-Grosse, M., Ghanashev, I., & Schlüter, M. (1997). Influence of transversal plasma density nonuniformity and collisions on surface wave propagation. Journal of electromagnetic waves and applications, 11(5), 609-632. https://doi.org/10.1163/156939397X00864

[26] Nowakowska, H., Zakrzewski, Z., & Moisan, M. (2001). Propagation characteristics of electromagnetic waves along a dense plasma filament. Journal of Physics D: Applied Physics, 34(10), 1474. https://doi.org/10.1088/0022-3727/34/10/307

[27] Zhang, W., Wu, L., Tao, J., & Huang, K. (2018). Numerical investigation of the gas flow effects on surface wave propagation and discharge properties in a microwave plasma torch. IEEE Transactions on Plasma Science, 47(1), 271-277. https://doi.org/10.1109/TPS.2018.2882637

[28] Dias, F. M., Tatarova, E., Henriques, J., & Ferreira, C. M. (1999). Experimental investigation of surface wave propagation in collisional plasma columns. Journal of applied physics, 85(5), 2528-2533. https://doi.org/10.1063/1.369570

[29] Tatarova, E., Dias, F. M., Ferreira, C. M., & Ricard, A. (1999). On the axial structure of a nitrogen surface wave sustained discharge: Theory and experiment. Journal of applied physics, 85(1), 49-62. https://doi.org/10.1063/1.369480

[30] Stafford, L. U. C., Margot, J., & Johnston, T. W. (2001). Propagation of surface waves in two-plasma systems bounded by a metallic enclosure. Journal of plasma physics, 66(5), 349-362. https://doi.org/10.1017/S0022377801001489

[31] Alves, L. L., Alvarez, R., Marques, L., Rubio, S. J., Rodero, A., & Quintero, M. C. (2009). Modeling of an axial injection torch. The European Physical Journal-Applied Physics, 46(2), 21001. https://doi.org/10.1051/epjap/2009049

[32] Rincón, R., Muñoz, J., & Calzada, M. D. (2015). Departure from Local Thermodynamic Equilibrium in argon plasmas sustained in a Torche à Injection Axiale sur Guide d'Ondes. Spectrochimica Acta Part B: Atomic Spectroscopy, 103, 14-23. https://doi.org/10.1016/j.sab.2014.11.005

[33] Snirer, M., Toman, J., Kudrle, V., & Jašek, O. (2021). Stable filamentary structures in atmospheric pressure microwave plasma torch. Plasma Sources Science and Technology, 30(9), 095009. https://doi.org/10.1088/1361-6595/ac1ee0.

[34] Rincón, R., Muñoz, J., Sáez, M., & Calzada, M. D. (2013). Spectroscopic characterization of atmospheric pressure argon plasmas sustained with the Torche à Injection Axiale sur Guide d'Ondes. Spectrochimica Acta Part B: Atomic Spectroscopy, 81, 26-35. https://doi.org/10.1016/j.sab.2012.12.006

[35] Rincón, R., Marinas, A., Muñoz, J., Melero, C., & Calzada, M. D. (2016). Experimental research on ethanol-chemistry decomposition routes in a microwave plasma torch for hydrogen production. Chemical Engineering Journal, 284, 1117-1126. https://doi.org/10.1016/j.cej.2015.09.062

[36] Casanova, A., Rincón, R., Muñoz, J., Ania, C. O., & Calzada, M. D. (2021). Optimizing high-quality graphene nanoflakes production through organic (bio)-precursor plasma decomposition. Fuel Processing Technology, 212, 106630. https://doi.org/10.1016/j.fuproc.2020.106630

[37] Toman, J., Šnírer, M., Rincón, R., Jašek, O., Vˇsianský, D., Raya, A.M., Muñoz, J., Calzada, M.D. (2023). On the gas-phase graphene nanosheet synthesis in atmospheric microwave plasma torch: Upscaling potential and graphene nanosheet-copper nanocomposite oxidation resistance. Fuel Processing Technology[Toman] Submitted. https://doi.org/10.1016/j.fuproc.2022.107534

[38] Tsyganov, D., Bundaleska, N., Tatarova, E., Dias, A., Henriques, J., Rego, A., ... & Phillips, J. (2015). On the plasma-based growth of 'flowing'graphene sheets at atmospheric pressure conditions. Plasma Sources Science and Technology, 239, 107534. https://doi.org/10.1088/0963-0252/25/1/015013

[39] Snirer, M., Kudrle, V., Toman, J., Jašek, O., & Jurmanová, J. (2021). Structure of microwave plasma-torch discharge during graphene synthesis from ethanol. Plasma

Sources Science and Technology, 30(6), 065020. https://doi.org/10.1088/1361-6595/abfbea

[40] Toman, J., Jašek, O., Šnírer, M., Pavliňák, D., Navrátil, Z., Jurmanová, J., ... & Michalička, J. (2021). On the transition of reaction pathway during microwave plasma gas-phase synthesis of graphene nanosheets: from amorphous to highly crystalline structure. Plasma Processes and Polymers, 18(8), 2100008. https://doi.org/10.1002/ppap.202100008

[41] Moussounda, P. S., Ranson, P., & Mermet, J. M. (1985). Spatially resolved spectroscopic diagnostics of an argon MIP produced by surface wave propagation (Surfatron). *Spectrochimica Acta Part B: Atomic Spectroscopy*, *40*(4), 641-651. https://doi.org/10.1016/0584-8547(85)80111-7

[42] Cotrino, J., Saez, M., Quintero, M. C., Menendez, A., Uria, E. S., & Medel, A. S. (1992). Spectroscopic determination of fundamental parameters in an argon microwave-induced plasma (surfatron) at atmospheric pressure. Spectrochimica Acta Part B: Atomic Spectroscopy, 47(3), 425-435. https://doi.org/10.1016/0584-8547(92)80035-F

[43] García, M. C., Yubero, C., Calzada, M. D., & Martínez-Jiménez, M. P. (2005). Spectroscopic characterization of two different microwave (2.45 GHz) induced argon plasmas at atmospheric pressure. Applied spectroscopy, 59(4), 519-528. https://doi.org/10.1366/0003702053641405

[44] Luque, J. M., Calzada, M. D., & Sáez, M. (2003). Experimental research into the influence of ion dynamics when measuring the electron density from the Stark broadening of the Hα and Hβ lines. Journal of Physics B: Atomic, Molecular and Optical Physics, 36(8), 1573. https://doi.org/10.1088/0953-4075/36/8/311

[45] Gigosos, M. A., Gonzalez, M. A., & Cardenoso, V. (2003). Computer simulated Balmer-alpha,-beta and-gamma Stark line profiles for non-equilibrium plasmas diagnostics. Spectrochimica Acta Part B: Atomic Spectroscopy, 58(8), 1489-1504. https://doi.org/10.1016/S0584-8547(03)00097-1

[46] Hrycak, B., Czylkowski, D., Jasiński, M., & Mizeraczyk, J. (2012). Tuning characteristics of coaxial microwave plasma source operated with argon, nitrogen and methane at atmospheric pressure. Electr. Rev, 88(11b), 310-2.

[47] Ricard, A., St-Onge, L., Malvos, H., Gicquel, A., Hubert, J., & Moisan, M. (1995). Torche à plasma à excitation micro-onde: deux configurations complémentaires. Journal de Physique III, 5(8), 1269-1285. https://doi.org/10.1051/jp3:1995185

[48] Gadonna, K., Leroy, O., Silva, T., Leprince, P., Boisse-Laporte, C., & Alves, L. L. (2011). Hydrodynamic study of a microwave plasma torch. The European Physical Journal-Applied Physics, 56(2), 24008. https://doi.org/10.1051/epjap/2011110161

[49] Leins, M., Schulz, A., Walker, M., Schumacher, U., & Stroth, U. (2008). Development and characterization of an atmospheric-pressure microwave plasma torch. IEEE transactions on plasma science, 36(4), 982-983. https://doi.org/10.1109/TPS.2008.924420

[50] Miotk, R., Hrycak, B., Jasiński, M., & Mizeraczyk, J. (2017). Characterization of an atmospheric-pressure argon plasma generated by 915 MHz microwaves using optical emission spectroscopy. Journal of Spectroscopy, 2017. https://doi.org/10.1155/2017/6359107

[51] Jonkers, J., Vos, H. V., Van der Mullen, J. A. M., & Timmermans, E. A. H. (1996). On the atomic state densities of plasmas produced by the “torche a injection axiale”. Spectrochimica Acta Part B: Atomic Spectroscopy, 51(5), 457-465. https://doi.org/10.1016/0584-8547(95)01450-0

[52] Jonkers, J., De Regt, J. M., Van der Mullen, J. A. M., Vos, H. P. C., De Groote, F. P. J., & Timmermans, E. A. H. (1996). On the electron temperatures and densities in plasmas produced by the “torche à injection axiale”. Spectrochimica Acta Part B: Atomic Spectroscopy, 51(11), 1385-1392. https://doi.org/10.1016/0584-8547(96)01493-0

[53] Jonkers, J., Hartgers, A., Selen, L. J. M., Van der Mullen, J. A. M., & Schram, D. C. (1999). The influence of nitrogen entrainment on argon plasmas created by theTorche à Injection Axiale'(TIA). Plasma Sources Science and Technology, 8(1), 49. https://doi.org/10.1088/0963-0252/8/1/006

[54] Zhu, W. C., Li, Q., Zhu, X. M., & Pu, Y. K. (2009). Characteristics of atmospheric pressure plasma jets emerging into ambient air and helium. Journal of Physics D: Applied Physics, 42(20), 202002. https://doi.org/10.1088/0022-3727/42/20/202002

[55] Calzada, M. D., Moisan, M., Gamero, A., & Sola, A. (1996). Experimental investigation and characterization of the departure from local thermodynamic equilibrium

along a surface-wave-sustained discharge at atmospheric pressure. Journal of applied physics, 80(1), 46-55. https://doi.org/10.1063/1.362748

[56] Moon, S. Y., & Choe, W. (2006). Parametric study of atmospheric pressure microwave-induced Ar⁄O2 plasmas and the ambient air effect on the plasma. Physics of plasmas, 13(10), 103503. https://doi.org/10.1063/1.2357722

[57] Tatarova, E., Dias, F. M., Henriques, J., & Ferreira, C. M. (2006). Large-scale Ar and N2–Ar microwave plasma sources. Journal of Physics D: Applied Physics, 39(13), 2747. https://doi.org/10.1088/0022-3727/39/13/018

[58] Bravo, J. A., Rincón, R., Muñoz, J., Sánchez, A., & Calzada, M. D. (2015). Spectroscopic characterization of argon–nitrogen surface-wave discharges in dielectric tubes at atmospheric pressure. Plasma Chemistry and Plasma Processing, 35(6), 993-1014. https://doi.org/10.1007/s11090-015-9647-4

[59] Ricard, A., Tetreault, J., & Hubert, J. (1991). Nitrogen atom recombination in high pressure Ar-N2 flowing post-discharges. Journal of Physics B: Atomic, Molecular and Optical Physics, 24(5), 1115. https://doi.org/10.1088/0953-4075/24/5/030

[60] Ricard, A., Pointu, A. M., Villeger, S., & Canal, C. (2010). Active species in N2 and N2-O2 afterglows for surface treatments. In Journal of Physics: Conference Series (Vol. 207, No. 1, p. 012006). IOP Publishing. https://doi.org/10.1088/1742-6596/207/1/012006

[61] Ricard, A., Besner, A., Hubert, J., & Moisan, M. (1988). High nitrogen atom yield downstream of an atmospheric pressure flowing Ar-N2 microwave discharge. Journal of Physics B: Atomic, Molecular and Optical Physics, 21(18), L579. https://doi.org/10.1088/0953-4075/21/18/006

[62] Mavadat, M., Ricard, A., Sarra-Bournet, C., & Laroche, G. (2011). Determination of ro-vibrational excitations of N2 (B, v′) and N2 (C, v′) states in N2 microwave discharges using visible and IR spectroscopy. Journal of Physics D: Applied Physics, 44(15), 155207. https://doi.org/10.1088/0022-3727/44/15/155207

[63] Kutasi, K., Sá, P. A., & Guerra, V. (2012). O2 dissociation in Ar–O2 surface-wave microwave discharges. Journal of Physics D: Applied Physics, 45(19), 195205. https://doi.org/10.1088/0022-3727/45/19/195205

[64] Sá, P. A., & Loureiro, J. (1997). A time-dependent analysis of the nitrogen afterglow in and-Ar microwave discharges. Journal of Physics D: Applied Physics, 30(16), 2320. https://doi.org/10.1088/0022-3727/30/16/010

[65] Boudam, M. K., Moisan, M., Saoudi, B., Popovici, C., Gherardi, N., & Massines, F. (2006). Bacterial spore inactivation by atmospheric-pressure plasmas in the presence or absence of UV photons as obtained with the same gas mixture. Journal of Physics D: Applied Physics, 39(16), 3494. https://doi.org/10.1088/0022-3727/39/16/S07

[66] Guerra, V., Tejero-del-Caz, A., Pintassilgo, C. D., & Alves, L. L. (2019). Modelling N2–O2 plasmas: volume and surface kinetics. Plasma Sources Science and Technology, 28(7), 073001. https://doi.org/10.1088/1361-6595/ab252c

[67] Van Gaens, W., & Bogaerts, A. (2013). Kinetic modelling for an atmospheric pressure argon plasma jet in humid air. Journal of Physics D: Applied Physics, 46(27), 275201. https://doi.org/10.1088/0022-3727/47/7/079502

[68] Loureiro, J., Guerra, V., Sá, P. A., Pintassilgo, C. D., & da Silva, M. L. (2011). Non-equilibrium kinetics in N2 discharges and post-discharges: a full picture by modelling and impact on the applications. Plasma Sources Science and Technology, 20(2), 024007. https://doi.org/10.1088/0963-0252/20/2/024007

[69] Nowakowska, H., Czylkowski, D., Hrycak, B., & Jasiński, M. (2021). Numerical and experimental analysis of radiation from a microwave plasma source of the TIAGO type. Plasma Sources Science and Technology, 30(9), 095011. https://doi.org/10.1088/1361-6595/ac1556

[70] Synek, P., Obrusník, A., Hübner, S., Nijdam, S., & Zajíčková, L. (2015). On the interplay of gas dynamics and the electromagnetic field in an atmospheric Ar/H2 microwave plasma torch. Plasma Sources Science and Technology, 24(2), 025030. https://doi.org/10.1088/0963-0252/24/2/025030

[71] Calzada, M. D., Garcıa, M. C., Luque, J. M., & Santiago, I. (2002). Influence of the thermodynamic equilibrium state in the excitation of samples by a plasma at atmospheric pressure. Journal of applied physics, 92(5), 2269-2275. https://doi.org/10.1063/1.1492869

[72] Martínez-Aguilar, J., González-Gago, C., Castaños-Martínez, E., Muñoz, J., Calzada, M. D., & Rincon, R. (2019). Influence of gas flow on the axial distribution of

densities, temperatures and thermodynamic equilibrium degree in surface-wave plasmas sustained at atmospheric pressure. Spectrochimica Acta Part B: Atomic Spectroscopy, 158, 105636. https://doi.org/10.1016/j.sab.2019.105636

[73] Munoz, J., & Calzada, M. D. (2008). Experimental research on surface wave Ar–He discharges at atmospheric pressure. Journal of Physics D: Applied Physics, 41(13), 135203. https://doi.org/10.1088/0022-3727/41/13/135203